Influence of the initial pressure and temperature on the explosion behavior of methane and hydrogen in pipings

A Auvray, J Daubech, C Proust, P Montagne

Influence of the initial pressure and temperature on the explosion behavior of methane and hydrogen in pipings

A. Auvray[1,2,3], J. Daubech[3], C. Proust[1,3], P. Montagne[2]

[1]Université de Technologie de Compiègne, Laboratory TIMR Compiègne, France
[2]General Electric Gas Power France, Belfort, France
[3]INERIS, Verneuil-en-Halatte, France

Abstract

Hydrogen is identified as a potential solution to decarbonize the energy sector, especially for gas turbine manufacturers. Although there are decades of experience using fuels with hydrogen in gas turbines, the increase of hydrogen content in fuel comes with a review of the risk scenario. This will ensure a safe transition from natural gas to hydrogen-hydrocarbon blended fuels use. The scenario treated in this study is related to a flame propagation in a long pipe, under high pressure and temperature. Existing experimental data and knowledge at these conditions are scarce and sometimes conflicting, and experiments have to be done. To choose the hardware and the instrumentation, a significant CFD-based analysis of the potential explosion effects was performed, and presented herein. The configuration is a 24m long and 100mm diameter closed straight pipe filled with a stoichiometric fuel-air mixture from ambient up to 200°C and 20 bar. As a fuel, pure hydrogen and pure methane were first considered, and then blends.

Keywords: hydrogen, methane, industrial pipes, flame propagation, initial pressure, initial temperature, CFD

I. INTRODUCTION

In the context of decarbonization, some gas power plants may be requested to switch from fossil fuels to hydrogen-hydrocarbon blended fuels. In addition, the multiplicity of electric equipment and the increase in renewable energy production challenge the stability of the electrical network. Gas turbines have strong advantages with regards to the flexibility and the power generated, and thus enable to equilibrate the electric production with consumption with a delay. That makes gas turbines an important assets for the future of the energy production. In this way, gas turbine manufacturers are interested in converting their current machines compatible with natural gas, to the use of hydrogen blends. While the system is designed following standards for natural gas use, these documents are still evolving with hydrogen, and the experience is limited. In order to get ready for H_2 gas turbines, risk scenarios are treated independently. Here the scenario of interest is a flame propagation in a long pipe. This environment is initially at high pressure and temperature. Catching the influence of initial conditions as pressure, temperature, and hydrogen content, is of interest to understanding hydrogen–hydrocarbon flame development in pipes, especially on the acceleration potential. This will help to develop knowledge for gas turbines' future design and process updates.

The literature shows only a few studies treating these process parameters' influence on flame propagation. Kuznetsov [1] highlighted the decrease of detonation run-up distance with pressure increase with hydrogen explosion experiments carried in 24m long and 105mm diameter pipe. Lohrer [2] reported a linear increase of explosion pressure with the initial pressure, but he did not observe flame speed variation. Ciccarelli [3] performed experiments in a 21m long and 270mm diameter pipe with annular rings distributed all along. He concluded that deflagration to detonation transition (also known as DDT) run-up distance decreases with initial temperature. This may be completed by the observation made by Sun [4] who noted a decrease in peak overpressure with an increase in initial temperature in a 50*50mm square cross section and 600m long duct.

In order to get experimental data at the gas turbine conditions of pressure and temperature, and to fill the literature gaps of knowledge, a new test rig has to be designed. This test rig will be 24m long and 100mm diameter to fit with gas turbines' characteristic geometry. The experimental activity will be performed at the INERIS laboratory. During the test rig design and sizing, it appeared reasonable to use a model that reproduces the effect of compression and flow on flame propagation (transients). This approach enabled to get more information on the expected phenomenon and get

quantitative results helpful to make technical choices. The present study aims at investigating the effect of initial pressure and temperature on the propagation of stoichiometric methane and hydrogen blends flames in the future experimental setup. CFD calculation was identified as well suited to get comparative trends, but due to the large spatial domain, the resolution of the flame was not realizable. Strong simplifications such as RANS formalism and combustion chemistry parametrize with constant laminar flame speed were necessary to reduce the cost of calculation. Thus, before performing the simulations of interest, preliminary simulations were carried out to adjust the solving parameters of the model, to match the results of past experiments performed with similar geometry. These are introduced in the first part of this study. Then, 10 cases of interest were calculated to examine the influence of initial pressure and temperature on hydrogen and methane flames in long pipes.

II. CALIBRATING THE NUMERICAL TOOL

The experiments used for the CFD calibration were performed in a 26m long, 100mm diameter straight steel pipe, closed at one end and open to the atmosphere at the opposite end [5]. Figure 1 shows the test rig.

The flammable mixture is prepared by the injection of air and fuel blend at the closed end and exiting at the open end, sweeping the entire pipe with this mixture. The air and fuel flow rates are regulated by two mass flowmeters, and the concentration is controlled with oxygen level measurement. The considered flammable mixtures are methane-air and hydrogen-air, both in stoichiometric proportions. The ignition is carried out using a heating wire that was identified as favoring the natural acceleration of the flame and producing reproducible results[5].
The metrology used for these tests includes pressure sensors, and photodiodes for flame position detection in the pipe.

Figure 1: Flame propagation test rig

The numerical model was developed and presented by Lecocq & al [6]. It is a CFD OpenFoam model built on a RANS formalism for the flow, considering the transport equations of species mass fraction, momentum, energy, and progress variable for the flame front modeling [7, 8]. This system is solved with the reactingFOAM pressure-based solver proposed by OpenFOAM [9]. The turbulence is implemented with $k-\omega SST$ model [10], considered as well suited for the confined environment.

The species mass fraction source term and progress variable source terms are closed using the following equations :

$$\bar{\rho}\widetilde{\dot{\omega}_c} = \rho_u S_L \Xi |\nabla \tilde{c}| \qquad (1)$$

$$\bar{\rho}\widetilde{\dot{\omega}_{Y_i}} = \bar{\rho}\widetilde{\dot{\omega}_c}(Y_i^b - Y_i^u) \qquad (2)$$

Where ρ_u is the unburned gas density, S_L is the laminar burning velocity, c is the progress variable, and Ξ is the wrinkling factor that increases the laminar burning velocity. This latter may be separated into two contributions that are the flame's interaction with turbulence Ξ_T, and the flame natural instabilities Ξ_I. The first one can be assessed from the Gülder correlation [11] presented in equation 3, while the second may be understood as a parameter representative of the natural flame instability. Indeed, it was observed experimentally that hydrogen flames, at low equivalence ratio, are unstable [3].

$$\Xi_T = 1 + 2c\Xi_{coeff}\sqrt{\frac{u'}{S_L}}R_\eta \qquad (3)$$

The wall law is used to capture the velocity gradient at the wall and to model the turbulence generation in this region. The chosen wall law is the one of Spalding [12] that allows continuity between the viscous sublayer, the buffer layer, and the turbulent region. The steel roughness is assumed to be 100 µm which is characteristic of a medium level of rust. The pipe end at the ignition is always considered as closed (boundary condition of stagnant flow) ; while the other end is considered as open (constant pressure $P_{ext} = 1\ atm$).

A first-order Euler scheme is applied to the time derivatives and second-order schemes for the space derivatives are used.

a) Mesh influence

The previous study carried out by Lecocq [6] assessed flame propagation in 24m long and 150mm diameter pipe. The diameter reduction to 100mm implied a new mesh generation for the present study. Four meshes were thus tested on the

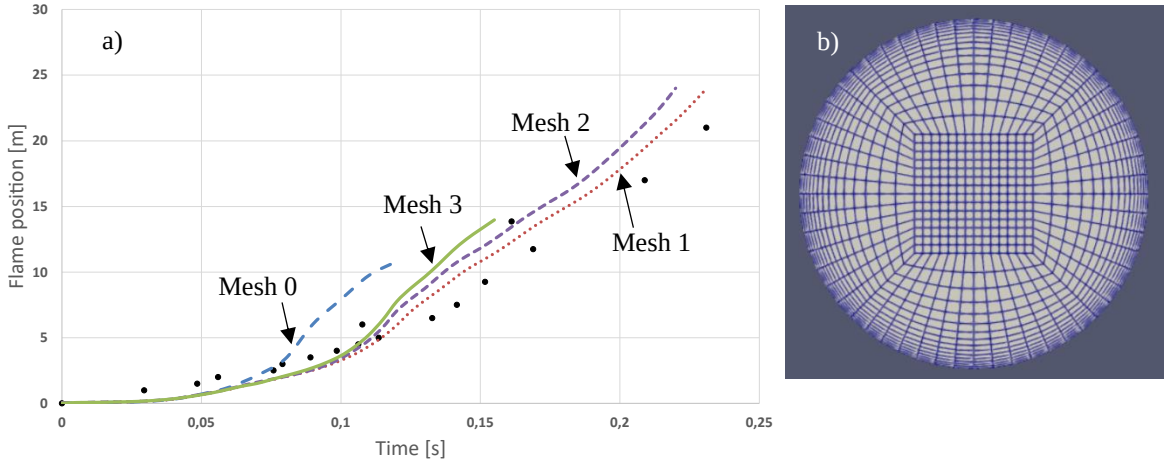

Figure 2: a) Mesh influence on the stoichiometric methane-air flame position in 26m long and 100mm diameter pipe. Dots are experimental measurements, lines are numerical simulations. b) view of the meshed pipe crossed section, with mesh 2

stoichiometric methane case. All meshes were hexahedral and were generated from the blockMesh function proposed by OpenFOAM. The comparison of the results is plotted on Figure 2.a, and the associated mesh characteristics are displayed in Table 1.

Table 1: Characteristics of the different tested mesh

	Mesh 0	**Mesh 1**	**Mesh 2**	**Mesh 3**
Number of cell	2,36M	2,64M	4,66M	5,3M
Internal square size (mm)	20	15	17	17
Maximum cell width at walls (mm)	1,21	0,75	0,68	0,61

Considering the slopes of the flame position curves, it appears that increasing the number of cells gives a slower flame between meshes 0 - 1, but the inverse trend is observed between meshes 1, 2, and 3. Because the variation of the position versus time curves between meshes 1, 2, and 3 is not so important, the chosen final mesh is mesh 2 for a compromise between precision, calculation cost (calculations with mesh 2 need 16 hours computation time for 0.25s physical time, while meshes 1 and 3 need respectively 8 and more than 20 hours) and homogeneous structure. The latter point must be understood as a minimized size variation for two nearby cells. For mesh 2, the maximum characteristic cell width is less than 6 mm, and the maximum cell aspect ratio is below 10. The cells are refined at the wall and allow to simulate the velocity profile in the boundary layer. Indeed, the non-dimensional normal distance of the cell to the wall, commonly called y+, is kept below 300 which is contained in the validated range of the Spading wall law.

b) Thermal boundary condition

The previous simulations in 150 mm diameter pipe were performed with adiabatic walls. The reduction from 150 mm to 100 mm implied for the present study increases the ratio of the external surface over the pipe volume, and thus, promotes the heat exchanges from burnt gas to walls. The assumption of constant temperature of walls can be considered valid regarding the Biot number of the pipe walls :

$$Bi = \frac{heat\ transfer\ in\ the\ wall}{heat\ transfer\ at\ wall\ surface} = \frac{hL_C}{\lambda} < 0.1 \qquad (4)$$

Where h, L_C and λ are respectively the heat transfer coefficient, the characteristic length, and the heat conductivity of the material.

Finally, the two values of Ξ_I in the progress variable source terms equation 1, were set to $\Xi_I = 1.0$ for the methane case, and $\Xi_I = 2.0$ for the hydrogen case. These values enabled to recover the experimental flame propagation with regard to the pressure and the flame position in time, as plotted on Figure 3.

III. PREDICTING THE INFLUENCE OF PRESSURE AND TEMPERATURE

For the parametric study, the whole model was conserved (mesh, equations, models, solver, etc.). The only change was the boundary condition at the opposite end from the ignition,

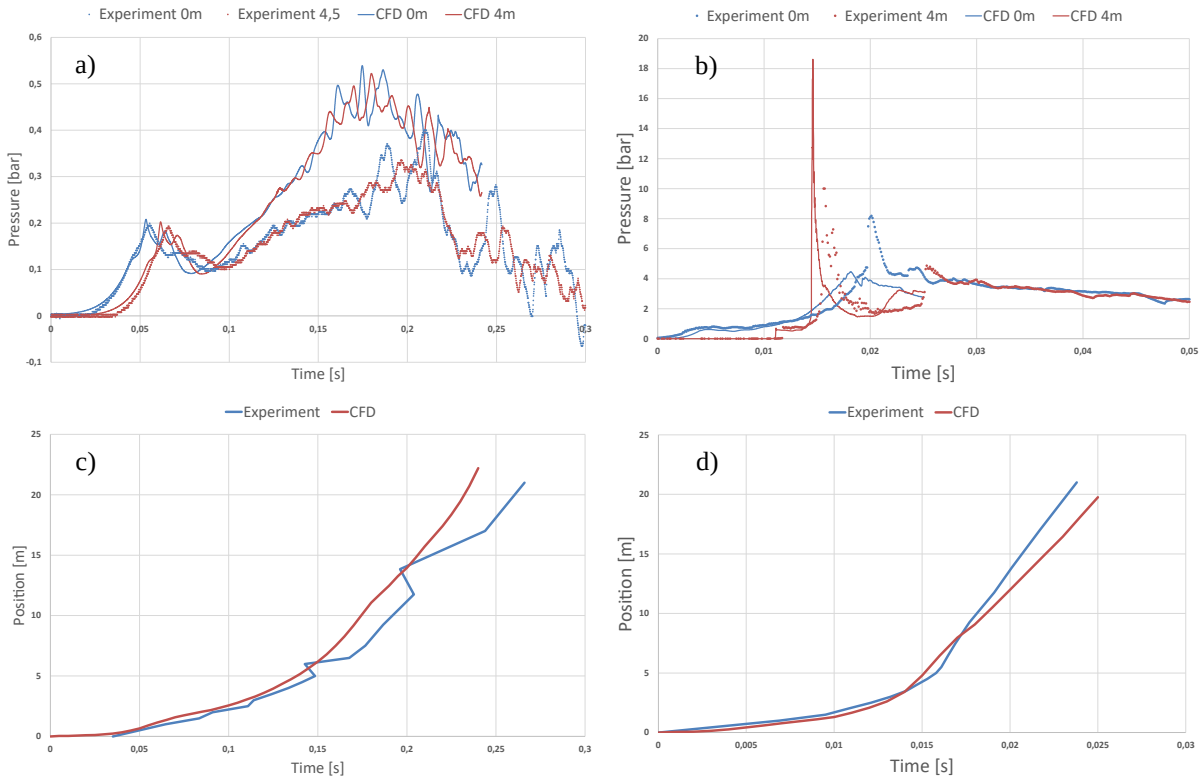

Figure 3: CFD modeling and experimental measurement comparison. a) pressure signal of CH_4-air flame at ignition and 4 m away from ignition, b) pressure signal of H_2-air flame at ignition and 4 m away from ignition, c) flame position of CH_4-air flame, d) flame position of H_2-air flame

Which was now considered as closed (stagnant flow). This configuration is representative of the future INERIS test rig.

The laminar burning velocity S_L used for the source term calculation equation 1, and the expansion rate σ (ie the ratio of unburnt over burnt gas densities), were calculated with Cantera [13], using the GRI3.0 mechanism. The results are presented in Table 2 for all tested conditions. It must be noted that this burning velocity is constant during the computation. As a results, neither the effect of reactant compression by the precursor pressure wave nor the temperature on reaction kinetic are accounted for. The latter especially concerns the flame extinction at the wall where the temperature is low.

a) Influence of initial temperature

The results for hydrogen-air and methane-air flame propagation with temperature at 1 bar initial pressure are plotted on Figure 4.

Table 2: Laminar flame speed values, and expansion rate for parametric cases

	H_2			CH_4		
Temperature (°C)	20	200	200	20	200	200
Pressure (bar)	1	1	20	1	1	20
Laminar flame speed (m/s)	2.25	4.8	2.44	0,36	0,81	0,23
Expansion rate σ (-)	7.01	4.53	4.67	7.66	4.95	5.07
$\sigma . S_L$ (m/s)	15.8	21.7	11.4	2.8	4	1.2

Looking at the hydrogen flame velocity curve in Figure 4.d, it appears that the flame propagates faster at the beginning when the temperature is high. This is in accordance with the increase in the product of laminar flame speed by the expansion rate (15.8 at 20°C and 21.7 at 200°C), which is usually considered as an intrinsic laminar propagation velocity. However, the flame slows down in the following

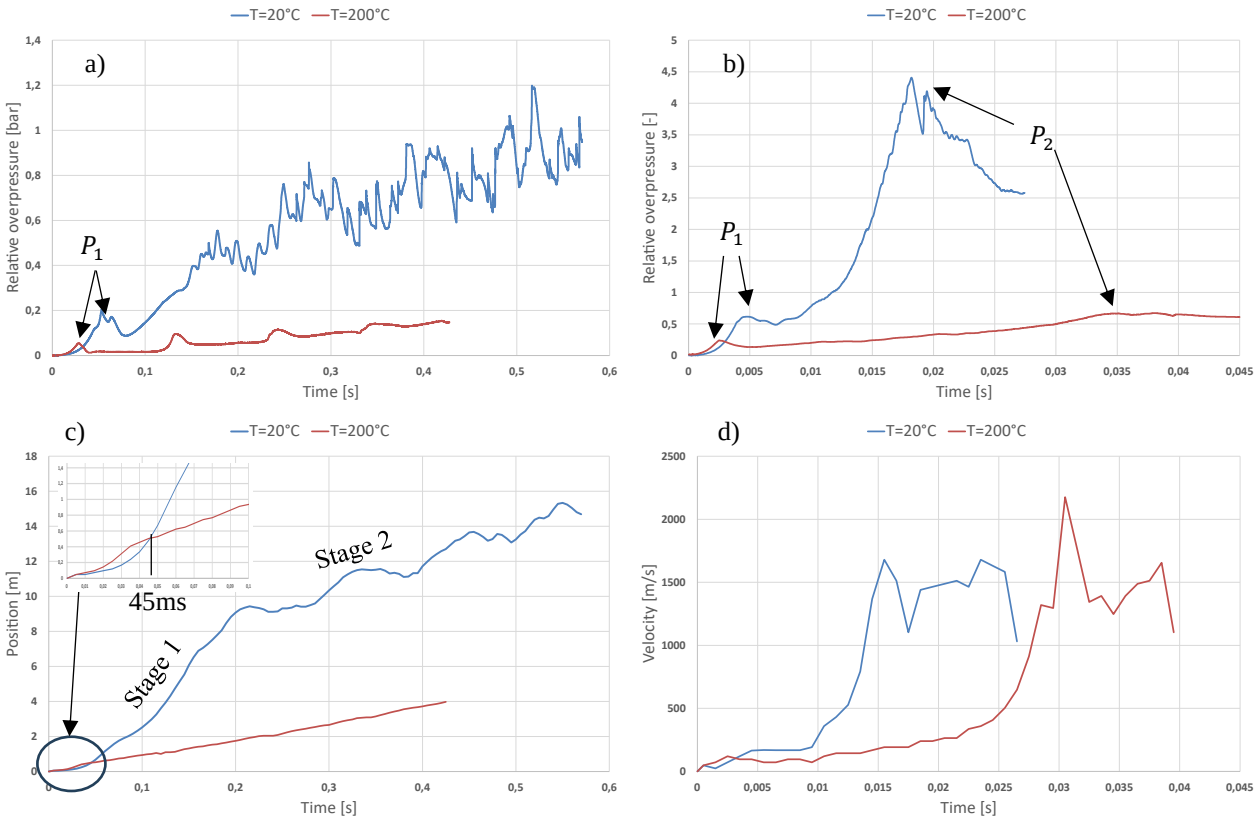

Figure 4: Temperature influence on flame propagation at atmospheric initial pressure. a) overpressure of methane-air flame, b) overpressure of hydrogen-air flame, c) methane-air flame position, d) hydrogen-air flame velocity

moments. On the pressure plot Figure 4.d, one may observe that the first pressure peak P_1 is reached earlier with the high-temperature test (4.8ms at 20°C and 2.7ms at 200°C). This first pressure peak is related to the partial extinction of the flame at the side walls [14]. Thus, the higher laminar propagation velocity of the flame under high temperature conditions might explain this earlier pressure peak. In both cases, the hydrogen flame undergoes a supersonic flame propagation, with velocities of the order of 1500m/s, that may be comparable to a detonation-like mode of propagation. Keeping in mind that no auto-ignition model was implemented in the code to be representative of the detonation propagation mechanism, the combustion mode of the flame here remains similar to a fast deflagration. This supersonic flame state is attained later with the higher temperature, and this is in contradiction with the DDT-promoting effect of temperature observed in long pipe with concentric rings [3]. The related pressure peak P_2 is largely lower with the high initial temperature condition, in accordance with the decrease of the volumetric energy density of the mixture.

For the case of methane, low initial temperature results in pressure and flame position periodic oscillations at 8.5Hz (resp. Figure 4.a and 4.c). In parallel, the pipe's natural frequency is equal to 7.3Hz according to equation 5.

$$f_0 = \frac{\sqrt{\gamma RT}}{2*L} \qquad (5)$$

Where γ is calculated for fresh gas, and L is the pipe length. These two frequencies let suggest a resonance of the pipe with excitation of the natural mode, and an oscillation of the flame front position as a response to the pipe acoustic, as observed in short pipe experiments [15, 16]. This behavior is assumed to be initiated by the reflected first pressure peak [16, 17], which meets the flame at approximately $0.190s$. It was stated in a previous study [17] that the following multiple flame-pressure waves interactions due to the pipe resonance structure the flame and increase its surface area. This might explain the distinction between the usual first exponential

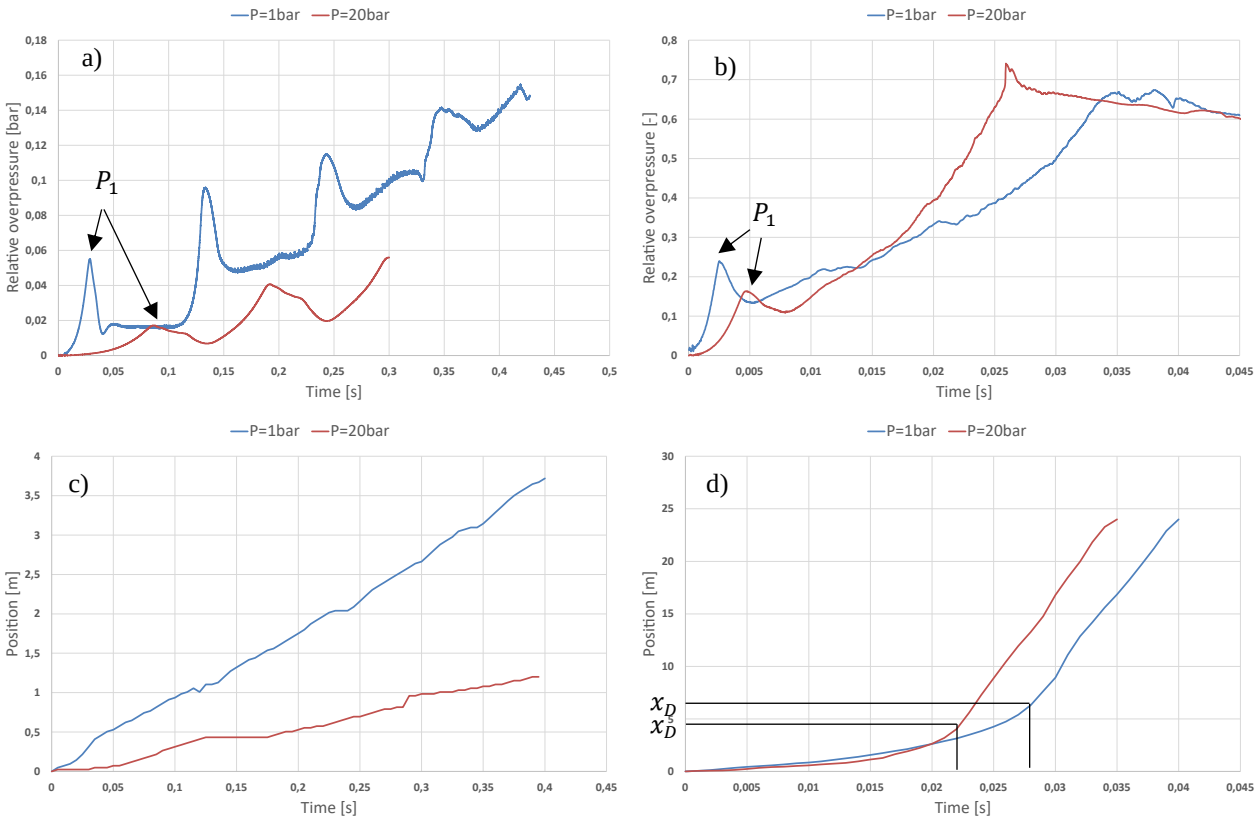

Figure 5: Pressure influence on flame propagation at 200°C initial temperature. a) overpressure of methane-air flame, b) overpressure of hydrogen-air flame, c) methane-air flame position, d) hydrogen-air flame position

flame development (stage 1) followed by the stage 2 of quite constant velocity (observed with the linear global slope of the position). The latter would be related to the "acoustic piloted" flame propagation.

The high-temperature flame behavior is different since the two stages flame development is replaced by a single linear flame propagation Figure 4.c. According to the initial slopes of the flame position curve, the flame would propagate faster in the first moment at high temperature, consistent with the $\sigma . S_L$ values (equal to 2.8 at 20°C and 4 at 200°C). But the position curves intersection at 45ms, and the slope of the curves in the following instants, reveal a lower global flame velocity. Looking at the pressure, we still observe oscillations at 9.2Hz, equal to the pipe's natural frequency, but the flame position doesn't respond the same way as in the low-temperature case. The amplitude of the initial pressure peak P_1 decreases with temperature. This signal might not be sufficient to disturb and structure the flame after the reflection at the wall. Nonetheless, the flame response to pressure waves interactions [18] is not implemented and should limit this conclusion.

b) Influence of initial pressure

Figure 5 shows the influence of initial pressure on the H_2-air and CH_4-air flames at 200°C initial temperature.

Starting with the case of hydrogen flame, it appears that the pressure decreases the first pressure peak P_1. The detonation-like regime is still reached for the case at 20 bar initial pressure, but at a distance $x_D = 4.5$ m from the ignition, compared to the $x_D = 6$ m at 1 bar. Thus, the distance to detonation decreases with pressure. This result supports the experimental observation with hydrogen-oxygen flames in a 24 m long pipe [1] but again the transition to detonation is not correctly handled in the code. About the generated overpressure relative to the initial pressure Figure 4.b, it appears that the case with high initial pressure gives a greater pressure rise for the second peak and suggests a greater flame acceleration.

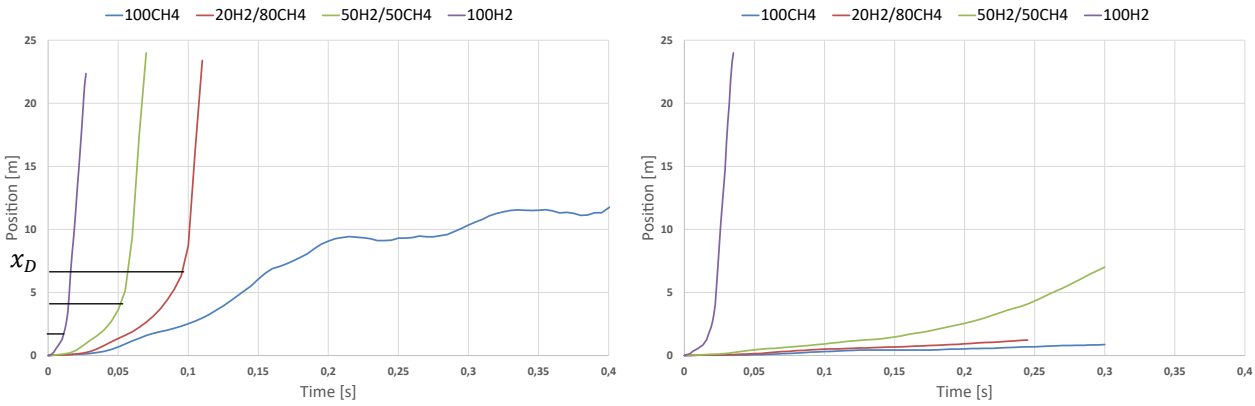

Figure 6: Flame position with time for 0, 20, 50 and 100% hydrogen concentration in methane. a) P=1bar, T=20°C ; b) P=20bar, T=200°C

The methane-air case position curve Figure 5.c shows a lower slope with the high-pressure case, which suggests a decrease of flame propagation velocity with initial pressure. Moreover, the transition from exponential to linear development occurs later, but at the same distance compared to the low-pressure case. Regarding the relative overpressure signal on Figure 5.a, pressure oscillations of large amplitude may be distinguished on both low and high-pressure curves with the same frequency (pipe's natural frequency). The amplitudes are proportional to the initial peak P_1, but still no flame position oscillations are noticeable.

c) H_2 and CH_4 blends

The computed flame propagations for 4 H_2-CH_4 blended fuels compositions are plotted on Figure 6. It appears on Figure 6.a) that the detonation-like state is reached for all fuels except methane. Thus, a behavior change would occur between 0% H_2 and 20% H_2. Also, the distance to reach the supersonic velocity (criterion for the DDT) decreases with the hydrogen content.

Looking on Figure 6.b), the H_2 / CH_4 blends are closer to the pure methane behavior since no supersonic flame propagation is noticeable. The combination of high pressure and temperature conditions would have an inhibiting effect on the flame propagation. As a result, the hydrogen content threshold for fast flame propagation would move in higher values, between 50 to 100% H_2.

IV. Conclusion and Perspectives

This numerical study precedes the experiments that will be performed in a new "long pipe" configuration test rig. The present numerical study was useful for the design, mechanical sizing, and sensor position choice of this latter test rig, as preliminary results.

CFD calculations were performed using a model previously developed and validated for methane-air and hydrogen-air flames under atmospheric conditions and in a 150mm diameter open pipe. To assess the effect of the initial conditions of pressure and temperature in a 100mm diameter closed pipe, the model and the mesh were somewhat changed, and calibrated from hydrogen-air and methane-air experiments carried out in this geometry. Extrapolations were made in initial pressure and temperature, and interpolations for the hydrogen content effect. The following conclusion can be made :

- The observation for a quick flame, as stoichiometric hydrogen-air, leads to a DDT-like promoting effect with increasing initial pressure and, inversely, a DDT inhibiting effect with increasing the initial temperature.
- The slower flame of methane seems to support the observation with hydrogen in terms of flame velocity, in a lesser manner since no transition to fast flame is observed. In addition, the methane flame propagation is mainly piloted by the acoustic of the pipe for low temperature and pressure conditions, with strong flame oscillations. This behavior vanishes with the increase in temperature.
- The hydrogen content threshold for fast flame and detonation-like propagation reaching is moved to higher values when the conditions of pressure and temperature are high.

These observations would be largely conditioned by the different limits of the model in these conditions. Three main identified limits are the constant $\boldsymbol{S_L}$, the lack of flame-pressure interaction submodel, and the Gülder correlation that is not validated for high-pressure and high-temperature

conditions and would need validation for confident use in such a CFD model.
The experimental campaign for the influence of pressure and temperature is expected to start in 2024 at the INERIS laboratory, in the framework of a PhD thesis. This would help to bridge the gap of experimental data needed to perform these simulations with confidence.

ACKNOWLEDGMENT

The author would like to thank the INERIS laboratory for sharing the experimental database from the BCRD research program used for the calibration of the model. The author is also grateful to Dr G. Lecocq, for his CFD experience sharing, and precious advice.

REFERENCES

[1] Kuznetsov et al. (2005) DDT in a smooth tube filled with a hydrogen-oxygen mixture. Shock Waves 14(3), pp. 205-215

[2] Lohrer, C., Drame, C., Schalau, B., Gr¨ atz, R., 2008. Propane/air deflagrations and cta measurements of turbulence inducing elements in closed pipes. J. Loss Prev. Process. Ind. 21, 1–10.

[3] Ciccarelli, G., Boccio, J. L., Ginsberg, T., Finfrock, C., Gerlach, L., Tagawa, H., & Malliakos, A. (1998). The effect of initial temperature on flame acceleration and deflagration-to-detonation transition phenomenon (No. NUREG/CR-6509; BNL-NUREG-52515). Brookhaven National Lab.(BNL), Upton, NY (United States); Nuclear Regulatory Commission, Div. of Systems Technology, Washington, DC (United States); Nuclear Power Engineering Corp., Tokyo (Japan).

[4] Sun, G., Deng, H., Xu, Z., Yan, M., Wei, S., Li, N., ... & Chen, G. (2023). Experimental and simulation study of NH3–H2-Air flame dynamics at elevated temperature in a closed duct. International Journal of Hydrogen Energy.

[5] Proust Ch. (2004). « Formation, inflammation, combustion des atmosphères explosives (ATEX) et effets associés », mémoire d'HdR présenté à l'Institut National Polytechnique de Lorraine, 12 février 2004.

[6] Lecocq, G., Daubech, J., & Leprette, E. (2023). Experimental and numerical study of the fuel effect on flame propagation in long open tubes. Journal of Loss Prevention in the Process Industries, 81, 104955.

[7] Poinsot, T., & Veynante, D. (2005). Theoretical and numerical combustion. RT Edwards, Inc..

[8] Wieland, C., Scharf, F., Schildberg, H. P., Hoferichter, V., Eble, J., Hirsch, C., & Sattelmayer, T. (2021). Efficient simulation of flame acceleration and deflagration-to-detonation transition in smooth pipes. Journal of Loss Prevention in the Process Industries, 71, 104504.

[9] Weller, H. G., Tabor, G., Jasak, H., & Fureby, C. (1998). A tensorial approach to computational continuum mechanics using object-oriented techniques. Computers in physics, 12(6), 620-631.

[10] Menter, F. R. (1994). Two-equation eddy-viscosity turbulence models for engineering applications. AIAA journal, 32(8), 1598-1605

[11] Gülder, Ö. L. (1991, January). Turbulent premixed flame propagation models for different combustion regimes. In Symposium (International) on Combustion (Vol. 23, No. 1, pp. 743-750). Elsevier.

[12] Spalding, D. B. (1961). A single formula for the law of the wall. Journal of Applied Mechanics, 28(3), 455-458.

[13] Goodwin, D. G., Moffat, H. K., & Speth, R. L. (2018). Cantera: An object-oriented software toolkit for chemical kinetics, thermodynamics, and transport processes. https://cantera.org/

[14] Bychkov, V., Akkerman, V. Y., Fru, G., Petchenko, A., & Eriksson, L. E. (2007). Flame acceleration in the early stages of burning in tubes. Combustion and Flame, 150(4), 263-276.

[15] Guenoche, H., & Markstein, G. H. (1964). Nonsteady flame propagation. Pergamon Press, New York, 107.

[16] Kerampran, S. (2000). Etude des mécanismes d'accélération des flammes se propageant depuis l'extrémité fermée vers l'extrémité ouverte de tubes horizontaux de longueur variable (Doctoral dissertation, Poitiers).

[17] Daubech, J. (2008). Contribution à l'étude de l'effet de l'hétérogénéité d'un prémélange gazeux sur la propagation d'une flamme dans un tube clos (Doctoral dissertation, Orléans).

[18] Chu, B. T. (1953, January). On the generation of pressure waves at a plane flame front. In Symposium (International) on Combustion (Vol. 4, No. 1, pp. 603-612). Elsevier.